Soft Matter

PAPER

View Article Online
View Journal | View Issue



Cite this: *Soft Matter*, 2026, **22**, 167

# Dynamic osmocapillary phase separation at contact lines

Qihan Liu * and Luochang Wang

Received 30th September 2025,
Accepted 26th November 2025

DOI: 10.1039/d5sm00993f

rsc.li/soft-matter-journal

When a drop of liquid is placed on top of a swollen solid, if the liquid is immiscible with the solvent of the swollen solid, the surface tension near the contact line can pull the solvent out from the solid, leading to a phase separation that converts the classical three-phase contact line into a four-phase contact zone. This phase separation can significantly affect the wetting properties of the swollen solid and the effect is known to be time dependent. This paper develops a dynamic osmocapillary model which predicts that the size of the phase separation increases with time, following the scaling relation of $t^{0.32}$. The prediction agrees well with existing experiments.



## 1. Introduction

Osmocapillary phase separation is a phenomenon where the surface tension pulls the solvent out from a swollen solid.[1–5] Here the swollen solid can be a hydrogel or a silicone elastomer, where the corresponding solvent would be water or unreacted silicone chains. When an immiscible liquid droplet sits on top of the swollen solid, the surface tension near the contact line can cause osmocapillary phase separation (Fig. 1). This phase separation can alter the wetting behavior,[6–11] which in turn affects applications such as coating, adhesion, antifouling, lubrication, *etc.*[12] The migration of the solvent out of the swollen solid is limited by the slow transport through the pore space of the swollen solid. Consequently, osmocapillary phase separation is often accompanied by noticeable time-dependent wetting behaviors. Existing observations include the sudden transition in droplet rolling speed and rate-dependent and time-dependent contact line deformation.[13–16]

Existing studies often model osmocapillary phase separation as an elastocapillary effect,[6,7,15–18] *i.e.*, the formation of the solvent phase is driven by surface tension and limited by the elasticity of the swollen solid. Then the flux towards the phase separation scales as $J \sim l_{EC}/\sqrt{t}$, where $l_{EC} = \gamma/\mu$ is the elastocapillary length, with $\gamma$ the surface tension and $\mu$ the shear modulus of the swollen solid.[15] Correspondingly, the size of phase separation grows with $\propto t^{1/2}$.[18] Alternatively, Cai *et al.* developed a phenomenological model that assumes the phase separation has a free energy quadratic in the volume of phase separation.[13] The model predicts no power law asymptote. In an earlier paper, we have shown that the equilibrium configuration of such phase separation at contact lines can be accurately predicted by the osmocapillary theory,[5] which provides a framework to rigorously model the dynamics of phase separation at contact lines without phenomenological assumptions or handwaving scaling arguments. This paper develops the dynamic osmocapillary model, which predicts that the size of phase separation grows with $\propto t^{0.32}$ when the associated elastic deformation is linear. This power law is quantitatively verified against existing experiments.

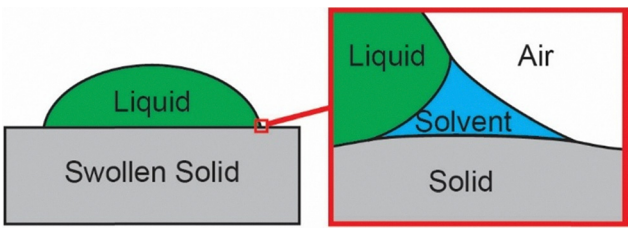


Fig. 1 Surface tension near the contact line can pull the solvent out from the swollen solid, causing osmocapillary phase separation.

## 2. General osmocapillary model polymeric gels

The migration of the solvent in a swollen solid is governed by the theory of poroelasticity. In polymeric gels, a nonlinear poroelastic model is often required to account for the large deformation. Here we adapt the model developed by Hong *et al.*[19] However, Hong's original formulation did not correctly identify the osmotic pressure. We will fix this issue and discuss the correct definition of osmotic pressure in a nonlinear poroelastic model.

A poroelastic model requires an elastic part describing the deformation and a kinetic part describing the solvent migration.

*Department of Mechanical Engineering and Materials Science, University of Pittsburgh, Pittsburgh, PA 15261, USA. E-mail: qihan.liu@pitt.edu*

The Flory–Rehner model is commonly used to describe the elastic response:

$$\sigma_{ij} = \frac{Nk_BT}{\det \mathbf{F}}\left(F_{jK}F_{iK} - \delta_{ij}\right) - p\delta_{ij}. \quad (1)$$

Here $\sigma_{ij}$ is the Cauchy stress tensor, $F_{iK}$ is the deformation gradient tensor relative to a stress-free dry reference state, $\det \mathbf{F}$ is the determinant of $F_{iK}$ reflecting the volume change of the gel, $N$ is the number of load-carrying polymer chains per unit of the reference volume, $k_BT$ is the product of Boltzmann constant and thermodynamic temperature. The reference state is taken as the dry polymer network. Since the shear moduli of gels ($<$10 MPa) are orders of magnitude lower than their bulk moduli ($\sim$GPa), gels deform incompressibly in most cases. Consequently, there will be a hydrostatic pressure $p$ that cannot be determined from the deformation using a constitutive model but rather must be determined from the boundary conditions.[19] Following the incompressible assumption, $\det \mathbf{F}$ and the local concentration of the solvent $C$ is connected through:[19]

$$\det(\mathbf{F}) = 1 + C\Omega. \quad (2)$$

Here $C$ is the number of solvent molecules per dry volume of the polymer network, $\Omega$ is the average volume per solvent molecule. The migration of the solvent in gel is often treated as diffusion:

$$j_i = -M_{ij}\frac{\partial \mu}{\partial x_j}. \quad (3)$$

Here $j_i$ is the diffusion flux vector, $M_{ij}$ is the mobility tensor, which generally depends on the deformation. $\mu$ is the solvent chemical potential in the solid. $\mu$ reflects the coupling between elasticity and the driving force for diffusion. According to the Flory–Rehner model:[19]

$$\mu = k_BT\left[\log\left(1 - \frac{1}{\det \mathbf{F}}\right) + \frac{1}{\det \mathbf{F}} + \frac{\chi}{(\det \mathbf{F})^2}\right] + p\Omega. \quad (4)$$

Here $\chi$ is a dimensionless parameter describing the mixing enthalpy.

In the study of osmocapillary phase separation, it is necessary to introduce the concept of osmotic pressure $\Pi$. In the context of physical chemistry, the osmotic pressure of a stress-free solution is defined as the pressure that need to be applied on the solution to resist the solvent absorption across a semi-permeable membrane (Fig. 2A).[20] In the context of the swelling of a polymeric gel, the osmotic pressure naturally generalizes to the pressure to prevent solvent absorption into the gel (Fig. 2B). This compressive pressure required to constrain the gel from swelling is the foundation of measuring gel osmotic pressure through the constrained swelling test.[21] Since both gel and solvent are incompressible in common practical conditions, applying a hydrostatic tension of the magnitude $\Pi$ over the whole system will not affect the thermodynamic equilibrium. Consequently, osmotic pressure $\Pi$ is also the tension in the solvent to resist the absorption of the gel (Fig. 2C). Take the

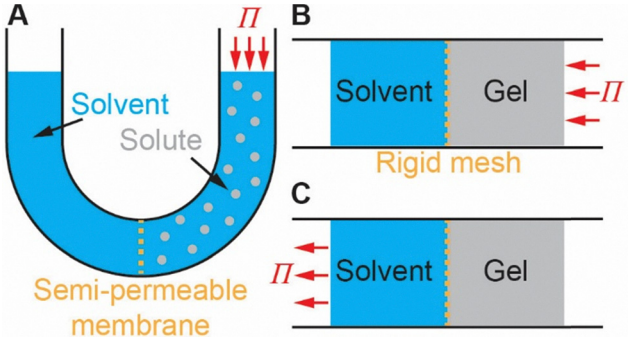


Fig. 2 The definition of osmotic pressure. (A) In a solution, the osmotic pressure $\Pi$ is defined as the pressure on the solution to resist solvent absorption. (B) In a polymeric gel, $\Pi$ is defined as the pressure on the gel to resist solvent absorption. (C) Since both solvent and gel are practically incompressible, $\Pi$ is also the tension in the solvent to resist absorption.

stress-free ambient solvent as the reference state for chemical potential $\mu = 0$. Since solvent molecules are treated as incompressible, moving one molecule from the stress-free reference state to the solvent under tension $\Pi$ induces a change in free energy of $-\Pi\Omega$. Then the chemical potential in the solvent of Fig. 2C is:

$$\mu = -\Pi\Omega. \quad (5)$$

This definition generalizes the osmotic pressure $\Pi$ to any stress state. Eqn (1)–(5) form the complete constitutive model for the poroelastic media.

There are six interfaces in the system: solid–liquid, solid–air, solid–solvent, solvent–air, solvent–liquid, and liquid–air. On each interface, the interfacial tension leads to the capillary pressure $p_C$. Following the Young–Laplace equation:[22]

$$p_C = \gamma\kappa. \quad (6)$$

Here $\gamma$ is the interfacial tension of the corresponding interface, $\kappa$ is the sum of the two principal curvatures. Since the solvent migration is slow, the solvent in the osmocapillary phase separation is always under static equilibrium, *i.e.* under uniform hydrostatic pressure $p_C$. To be consistent with the assumption of incompressible gel, the solvent must also be treated as incompressible, then the chemical potential in this solvent phase is:

$$\mu = p_C\Omega. \quad (7)$$

Combine eqn (7) with eqn (5) we have $-p_C = \Pi$ on the solid–solvent boundary, meaning that the capillary pressure pulling the solvent out from the solid and the osmotic pressure pulling the solvent into the solid balances each other. To determine the size of the osmocapillary phase separation, Neumann's law must be satisfied at the three-phase contact lines:[23,24]

$$\gamma_1\mathbf{n_1} + \gamma_2\mathbf{n_2} + \gamma_3\mathbf{n_3} = 0. \quad (8)$$

Here 1, 2, 3 refer to the three interfaces at the contact line. $\mathbf{n_i}$ is the unit vector normal to the contact line while tangent to the

 

corresponding interface. Since the stress state and chemical potential of the solvent in the osmocapillary phase separation can be explicitly written out, this solvent phase does not need to be explicitly modeled. One only needs to apply eqn (6) as the traction boundary condition and eqn (7) as the chemical potential boundary condition on the solid phase.

## 3. Linearized osmocapillary model for polymeric gels

In addition to pulling the solvent out from the gel and resulting in osmocapillary phase separation, the surface tension at the contact lines can also deform the gel resulting in elastocapillary deformation.[25,26] Osmocapillary phase separation and elastocapillary deformation are competitive phenomena. As the surface tension tries to deform a solid surface, the deformation can happen through either deforming the solid, *i.e.* elastocapillary deformation, or pulling out the solvent, *i.e.* osmocapillary phase separation. When one phenomenon is significant, the other is negligible.[2–5] Consequently, if we focus on the cases of significant osmocapillary phase separation, we can assume small deformation to linearize the problem.

Take an isotropic swollen state as the reference state, the general incompressible nonlinear poroelastic constitutive relation (eqn (1)–(5)) can be linearized into (Appendix 1):

$$\sigma_{ij} = 2G\left(\varepsilon_{ij} - \frac{\varepsilon_{kk}}{3}\delta_{ij}\right) + K\varepsilon_{kk}\delta_{ij} + \hat{\Pi}\delta_{ij}. \tag{9}$$

Here $\varepsilon_{ij}$ is the linear strain tensor, $G$ and $K$ are the shear and bulk moduli with the expressions:

$$G = \frac{Nk_BT}{(\det \mathbf{F})^{1/3}}, \tag{10}$$

$$K = Nk_BT\frac{3-(\det \mathbf{F})^{2/3}}{3\det \mathbf{F}} + \frac{k_BT}{\Omega}\left[\frac{1}{\det \mathbf{F}-1} - \frac{1}{\det \mathbf{F}} - \frac{2\chi}{(\det \mathbf{F})^2}\right], \tag{11}$$

$\hat{\Pi}$ is the change in osmotic pressure relative to the isotropic swollen reference state. $\hat{\Pi}$ is equivalent to the pore pressure in the classical linear poroelastic model but with a negative sign.[27] The isotropic swollen reference state is stress-free, with the corresponding reference osmotic pressure:

$$\begin{aligned}\Pi_0 = &-\frac{Nk_BT}{\det \mathbf{F}}\left((\det \mathbf{F})^{2/3}-1\right)\\ &-\frac{k_BT}{\Omega}\left[\log\left(1-\frac{1}{\det \mathbf{F}}\right)+\frac{1}{\det \mathbf{F}}+\frac{\chi}{(\det \mathbf{F})^2}\right].\end{aligned} \tag{12}$$

Eqn (2) becomes:

$$\varepsilon_{kk} = \Omega(c - c_0) \tag{13}$$

Here $c_0$ is the solvent concentration in the undeformed swollen state. Since the reference state is isotropic, the mobility tensor $M_{ij}$ should also be isotropic, then the law of solvent migration (eqn (3)–(5)) becomes:

$$j_i = M\Omega\frac{\partial \hat{\Pi}}{\partial x_i} \tag{14}$$

Here $M$ is the mobility. At the same time, Darcy's law predicts that the volumetric flux of the solvent $\mathbf{q}$ follows:

$$q_i = \frac{k}{\eta}\frac{\partial \hat{\Pi}}{\partial x_i} \tag{15}$$

Here $k$ is the permeability of the porous media, which generally depends on the swelling ratio.[28] $\eta$ is the viscosity of the solvent. Since $q_i = j_i\Omega$, eqn (15) and (16) require:

$$\frac{k}{\eta} = M\Omega^2. \tag{16}$$

The linear poroelastic model has two dimensionless groups, $K/G$ governs the compressibility of the network when solvent can drain freely. Note that this compressibility does not conflict with the incompressibility of the solvent and the undrained gel. $\Pi_0/G$ governs the capability for osmotic pressure to deform the solid. Here $\Pi_0$ is the osmotic pressure in the undeformed swollen state. If $\Pi_0/G \gg 1$, it is easier to deform the solid rather than pulling out the solvent, then osmocapillary phase separation will be insignificant. $\Pi_0$ can be directly written out. Eqn (10)–(12) connect $K/G$ and $\Pi_0/G$ in the linear poroelastic model with the parameters of the nonlinear Flory–Rehner model. Here the parameters of the Flory–Rehner model form three dimensionless groups: the swelling ratio $\det \mathbf{F}$, $N\Omega$ describes the relative strength of network elasticity and polymer–solvent mixing, and $\chi$ describes the relative strength of the enthalpy and entropy in polymer–solvent. We plot $K/G$ and $\Pi_0/G$ as a function of swelling ratio $\det \mathbf{F}$ for common ranges of $N\Omega$ and $\chi$ from the dry state to the fully swollen state (Fig. 3A and B). At a low swelling ratio, $K/G \gg 1$, indicating the network is nearly incompressible even when the solvent is allowed to drain freely. As the gel approaches the fully swollen state, $K/G \sim 1$. At a low swelling ratio, $\Pi_0/G \gg 1$, meaning that it is easier to deform the gel than pulling the solvent out. Consequently, osmocapillary phase separation will be negligible. As the gel approaches the fully swollen state, $\Pi_0/G \to 0$, meaning that it is easier to cause osmocapillary phase separation rather than deforming the gel. Consequently, elastocapillary deformation will be negligible. If we plot $K/G$ against $\Pi_0/G$ (Fig. 3C), we see that when osmocapillary phase separation is significant ($\Pi_0/G < 1$), $K/G$ is nearly a constant on the order 1. Since Flory–Rehner model could not accurately predict the swelling behavior of real polymer networks,[21] the exact value of $K/G$ predicted by the model may not be accurate. Nevertheless, the basic trends and the order-of-magnitude behavior in Fig. 3 should be trustable.

The osmocapillary model has two intrinsic length scales, the osmocapillary length $l_{OC} = \gamma/\Pi_0$ and the elastocapillary length $l_{EC} = \gamma/G$.[2–5] Osmocapillary length represents the length scale over which surface tension can cause osmocapillary phase

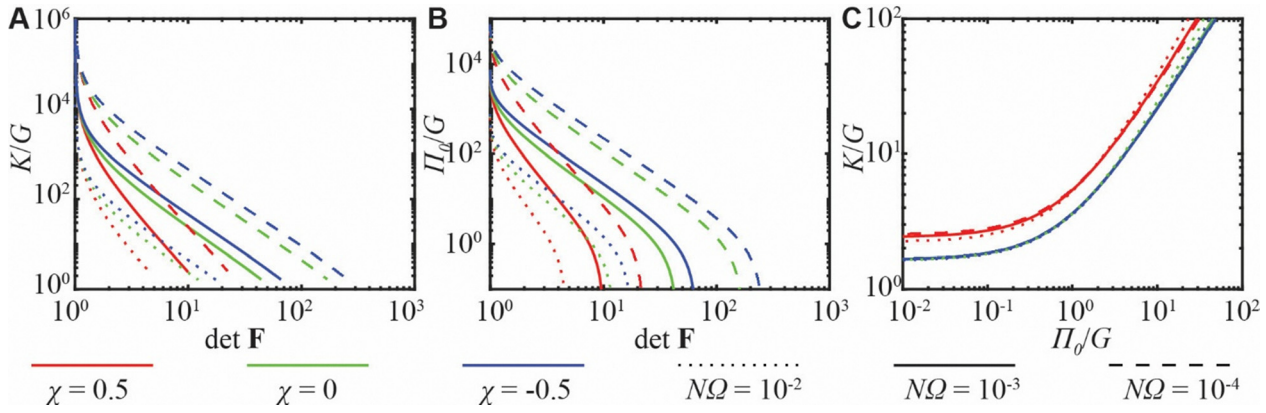


Fig. 3 The correspondence between nonlinear and linear poroelastic models. (A) How the network compressibility $K/G$ depends on swelling. All curves end at the fully swollen states. (B) How the osmotic pressure depends on swelling. All curves end at $\Pi/G = 0$ when the gel is fully swollen. (C) The $K/G$–$\Pi_0/G$ relation shows that $K/G \sim 1$ when the osmocapillary effect is significant ($\Pi_0/G < 1$).

separation. Elastocapillary length represents the length scale over which surface tension can significantly deform the swollen solid. These two length scales lead to two poroelastic relaxation times, the osmocapillary relaxation time, $t_{OC} = {l_{OC}}^2\eta/kG$, and the elastocapillary relaxation time $t_{EC} = {l_{EC}}^2\eta/kG$. Here $kG/\eta$ has the dimension of diffusivity. These length and time scales will be used to normalize the simulation results in the following sections.

## 4. Numerical model of osmocapillary phase separation at contact lines

We will numerically analyze the osmocapillary phase separation at contact lines (Fig. 1), which is the most common configuration to observe osmocapillary phase separation.[6,7,16–18] We make two assumptions to simplify the problem:

(1) In most cases, the size of phase separation is much smaller than the size of the droplet and the dimension of the porous solid. Then the curvatures of the droplet and the solid are negligible at the scale of phase separation. The phase separation can be modeled as a 2D plane-strain problem on a flat semi-infinite porous media.

(2) We limit the discussion to the cases where osmocapillary phase separation dominates over the elastocapillary deformation ($\Pi_0/G < 1$), the deformation in the gel is negligible. Then the swollen solid surface remains flat as osmocapillary phase separation grows. There is no capillary pressure on the flat surface. Also, the small deformation ensures that the linearized model can be used.

Under these two simplifications, the geometry of osmocapillary phase separation can be analytically determined (Appendix 2), with the width $w = C_w\gamma/p_C$, height $h = C_h\gamma/p_C$, and volume $V = C_V(\gamma/p_C)^2$ connected to the solvent–air interfacial energy $\gamma$ and the capillary pressure in the solvent phase $p_C$. Here $C_w$, $C_h$, and $C_V$ are constants that depend on the interfacial energies of the six interfaces involved. These relations allow us to track a single variable $p_C$ for the evolution of osmocapillary phase separation.

The evolution of the osmocapillary phase separation is governed by the conservation of mass:

$$\frac{dV}{dt} = \int_0^w q_y dx \tag{17}$$

Here the integration is over the boundary of the swollen solid covered by osmocapillary phase separation. Using the relation between $w$, $h$, $V$, and $p_C$, eqn (17) can be converted into an ordinary differential equation of the capillary pressure $p_C$:

$$-2C_V\frac{\gamma^2}{{p_C}^3}\frac{dp_C}{dt} = \int_0^{C_w\gamma/p_C} q_y dx \tag{18}$$

In eqn (18), if we rescale time with $\hat{t} = t/C_V$ and length with $\hat{x} = C_w x$, the factors $C_V$ and $C_w$ are gone, meaning that these geometry-dependent factors do not affect the nature of the relaxation. Without loss of generality, we set $C_V = C_w = C_h = 1$ in our study.

Note that eqn (17) only describes the growth of an existing osmocapillary phase separation. It does not describe the nucleation of an osmocapillary phase separation from a flat surface. Consequently, an initial phase separation width $w_0$ must be introduced in the simulation as an initial condition. This is equivalent to placing a line of solvent on a piece of homogeneous gel at $t = 0$. This initial condition will affect the dynamics of phase separation when the current phase separation width $w \sim w_0$. When $w \gg w_0$, the effect of initial condition is negligible, and the simulation reflects the universal dynamics of osmocapillary phase separation.

We implement the above problem in the finite element analysis package COMSOL 6.3. The simulation domain and boundary conditions are schematically represented in Fig. 4A. Taking advantage of the symmetry, we only simulate half of the poroelastic media, where the capillary pressure is applied over the surface from 0 to $w/2$. Note that the osmocapillary phase separation on top of the solid phase may not be symmetric, as schematically illustrated in Fig. 1B. However, since we assumed small deformation, the solvent phase only applies a uniform pressure over a segment of the flat surface of the solid phase.

 

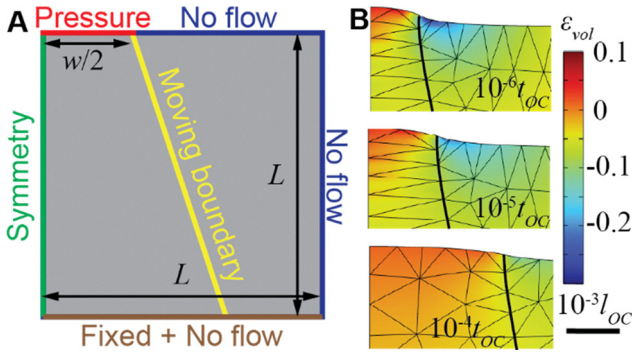


Fig. 4 (A) The schematic of the simulation setup. Only the swollen solid is simulated. The interaction with the solvent phase is reflected through the pressure boundary condition (red). (B) Snapshots of the simulation showing how the moving boundary (thick black line) is shifted horizontally to represent the widening of the osmocapillary phase separation. Thin solid lines represent the element boundaries. Remeshing was performed between $10^{-5}t_{OC}$ and $10^{-4}t_{OC}$. $\varepsilon_{vol}$ is the volumetric strain, which in the incompressible case represents the volume of solvent exchange. $K/G = 1$. $\Pi_0/G = 10^{-3}$.

The uniform pressure over flat surface is symmetric. Note that at the isotropic swollen reference state, the solid is stress-free but has a finite osmotic pressure. Consequently, over the pressure boundary, the stress driving the deformation is the total capillary pressure (eqn (6)) relative to 0 stress. The pressure driving the solvent migration is the difference between the capillary pressure and the reference osmotic pressure $\Pi_0$. And this pressure difference can be implemented either by adjusting the reference pressure in the bulk or the applied pressure on the boundary. We implemented it by adjusting the reference pressure because the other implementation is numerically less stable in COMSOL.

We set the size of the simulation domain $L \gg w$ to approximate semi-infinite space. Since we assume small deformation, the flat surface remains flat, there is no capillary pressure on the boundaries. The growth of osmocapillary phase separation implies that the width of the pressure boundary condition, $w/2$, needs to widen during the simulation. We implement this time-dependent boundary condition by deforming the mesh relative to the solid domain. A sloped line from the edge of the phase separation to the bottom of the simulation domain is defined as a moving boundary to deform the mesh. This line is shifted uniformly rightward during the simulation to represent the growth in the phase separation width $w$ (Fig. 4B). The line ensures that the mesh is uniformly stretched and compressed on both sides. In contrast, if we only shift the boundary point, the mesh will be locally distorted.

The governing equations of the swollen solid outlined in Section 3 are implemented using the built-in poroelasticity module. The changing width of osmocapillary phase separation is modeled as a moving boundary using the deformed geometry module. The evolution equation of the osmocapillary phase separation (eqn (18)) is implemented through the global ODE and DAE module. The domain is discretized with quadratic triangle elements for all modules. We set the element size to be $w_0/6$ at the edge of the osmocapillary phase separation. The element gradually coarsens to $20l_{OC}$ far from the region of osmocapillary phase separation. The simulation is regularly remeshed to avoid element distortion associated with the moving boundary (Fig. 4B). We set $w_0/2 = 10^{-3}l_{OC}$ at $t = 0$ as the initial condition. An example simulation file is provided as SI. For this initial phase separation size, the capillary pressure $p_C$ will be $10^3\Pi_0$, which can lead to large deformation at short time scales. At long time scales, $\Pi_0/G < 1$ ensures small deformation. We maintain the linear poroelastic treatment at all time scales so that any deviation from the model indicates the nonlinear effect. We perform the simulation from $t = 10^{-5}t_{OC}$ to $t = 10^5 t_{OC}$. We limit the first time step to be much less than the relaxation time associated with $w_0$, $w_0^2\eta/kG$, to accurately resolve the initial response. The simulation domain size is fixed to $L = 300l_{OC}$, which ensures that the osmotic pressure $\Pi$ in the swollen solid is negligibly affected (<1%) by the solvent removed by osmocapillary phase separation. In the true semi-infinite limit, $\Pi$ should not be affected by the phase separation. Recall that $w = C_w\gamma/p_C$ and $p_C = -\Pi$ at equilibrium, then <1% change in $\Pi$ implies <1% error in $w$ compared to the semi-infinite limit.

## 5. The growth dynamics of osmocapillary phase separation

We first compare the simulation of different $\Pi_0/G < 1$ at fixed $K/G = 1$, consistent with the Flory–Rehner model in Fig. 3 by the order of the magnitude. If we use osmocapillary length $l_{OC} = \gamma/\Pi_0$ and osmocapillary relaxation time $t_{OC} = l_{OC}^2\eta/kG$ for normalization (Fig. 5A), the results show that cases with different $\Pi_0/G$ approaches the same equilibrium osmocapillary phase separation size, indicating that the equilibrium phase separation size is governed by the osmocapillary length $l_{OC}$ as expected. The case with larger $\Pi_0/G$ reaches equilibrium faster because a higher $\Pi_0$ means a steeper gradient $\partial\Pi/\partial x_i$ can form in the solid, which results in a larger flux $q_i$ according to eqn (14), and a larger flux means a faster growth of the osmocapillary phase separation.

If we normalize the results using elastocapillary length $l_{EC} = \gamma/G$ and elastocapillary relaxation time $t_{EC} = l_{EC}^2\eta/kG$, we see that all cases follow the same relaxation asymptotic at short time (Fig. 5B), indicating the relaxation dynamics is independent of the stress-free osmotic pressure $\Pi_0$. Relaxation at the short time scale follows the power law $w \propto t^{0.32}$. This power law can be interpreted through the following scaling analysis. Here we use "$\propto$" to indicate "proportional to". Since $V \propto w^2$, eqn (17) leads to:

$$w\mathrm{d}w \propto wq_y\mathrm{d}t. \tag{19}$$

Recall eqn (15), $q_y \propto \partial\Pi/\partial\gamma$. We can estimate the difference in $\Pi$ by the capillary pressure $\gamma/w$ and the length scale of diffusion as $w$, then $\partial\Pi/\partial\gamma \propto \gamma/w^2$. That is:

$$q_y \propto \gamma/w^2. \tag{20}$$

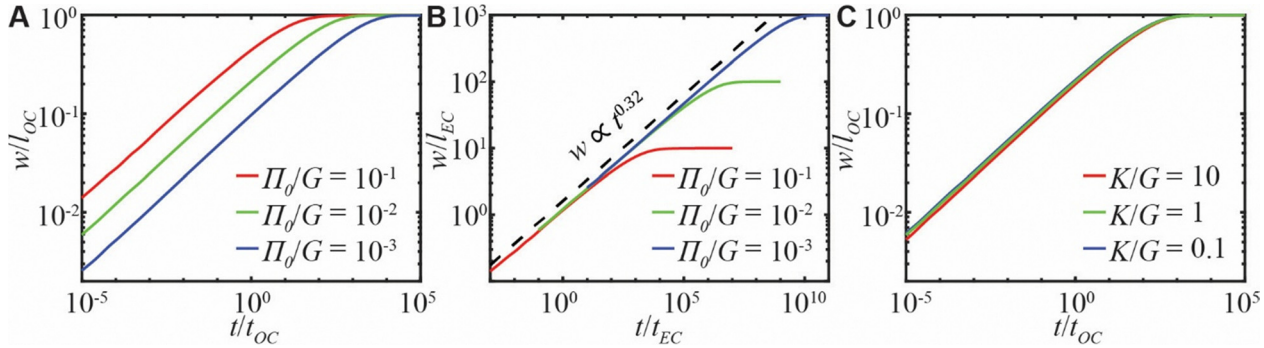


Fig. 5 How the width of osmocapillary phase separation increases with time (A) fixing $K/G = 1$, normalization with osmocapillary length $l_{OC} = \gamma/\Pi_0$ and relaxation time $t_{OC} = l_{OC}^2\eta/kG$ shows that the equilibrium osmocapillary phase separation size is governed by $l_{OC}$. (B) Fixing $K/G = 1$, normalization with elastocapillary length $l_{EC} = \gamma/G$ and relaxation time $t_{EC} = l_{EC}^2\eta/kG$ shows that the relaxation dynamics is unaffected by $\Pi_0/G$. (C) Fixing $\Pi_0/G = 10^{-2}$, results show that network compressibility has little affect on the relaxation dynamics.

Combining eqn (19) and (20), we can integrate to:

$$w^3 \propto t. \tag{21}$$

This corresponds to $w \propto t^{0.33}$. The difference between $t^{0.33}$ and $t^{0.32}$ could be due to the negligence of the inhomogeneous flux field in the estimation. This is scaling is different from the classical scaling of Fickian diffusion,[29] which predicts a $t^{0.5}$ power law for increasing length scales. The difference between $t^{0.33}$ and $t^{0.5}$ is caused by the evolving boundary pressure and boundary width in osmocapillary phase separation. Under this normalization, the difference in equilibration time is more significant compared to Fig. 5A. This is because under this normalization, higher $\Pi_0/G$ also implies a smaller volume of equilibrium phase separation $V_0 \propto (\gamma/\Pi_0)^2 = l_{OE}^2(\Pi_0/G)^{-2}$ to diffuse out from the solid.

Next, we compare the simulation of different $K/G$ with fixed $\Pi_0/G = 10^{-2}$. It turns out that the compressibility of the polymer network only weakly affects the relaxation of osmocapillary phase separation (Fig. 5C), indicating that the osmocapillary relaxation time $t_{OC} = l_{OC}^2\eta/kG$ is a good time scale for normalization. When $K/G$ is varied between 0.1 to 10, there is only about 10% change in the osmocapillary phase separation size $w$ at a fixed time $t$. Note that the hydraulic diffusivity due to poroelastic effect, $D = (K + 4G/3)k/\eta$, is sensitive to $K/G$.[30] However, while a higher network bulk modulus $K$ leads to faster diffusion, it also limits the volumetric change of the swollen solid. Then a gentler gradient of solvent content slows down the solvent diffusion. Since the total volume of osmocapillary phase separation is not affected by $K/G$, these two effects largely cancel out so that osmocapillary relaxation time is insensitive to $K/G$.

## 6. The elastic deformation induced by osmocapillary phase separation

Unlike the growth of osmocapillary phase separation, which approaches a size-independent behavior in the limit of semi-infinite space, the elastic deformation induced by osmocapillary phase separation keeps increasing with the domain size. This size dependence is a well-established behavior of a linear elastic semi-infinite space subject to a surface pressure distribution.[31] Here we will not discuss the dependence on the domain size and will simply fix $L = 300l_{OC}$. We take the difference of the upward displacements between the top-left and top-right corners of Fig. 4 in simulation to characterize the elastic deformation induced by osmocapillary phase separation. This difference represents the deformation under the osmocapillary phase separation relative to the far field. We denote this difference with symbol $H$.

We first compare the simulation of different $\Pi_0/G$ at fixed $K/G = 1$. Here normalizing using the osmocapillary length $l_{OC} = \gamma/\Pi_0$ is equivalent to normalizing using the simulation domain size because we fix $L = 300l_{OC}$. We see the higher $\Pi_0/G$ leads to larger elastic deformation (Fig. 6A). By linear elasticity, the displacement is linearly proportional to $\Pi_0/G$. If we further normalize $H$ with $\Pi_0/G$, we see all cases converge at the short and long time scales (Fig. 6B), corresponding to the undrained and drained limits. Here the case of $\Pi_0/G = 10^{-3}$ slightly deviates from the other cases at the drained (long-time) limit because the magnitude of $H$ is so small before normalization (recall Fig. 6A) that the slight deswelling of the solid due to osmocapillary phase separation becomes non-negligible. If the comparison were done using an even larger simulation domain, the deviation should disappear. At the intermediate time, all cases show $H$ first decreases then increase. This is because initially osmocapillary phase separation locally drains solvent thus causing temporary deswelling. Near equilibrium, osmocapillary phase separation ceases to pull out solvent. Then surrounding solvent can replenish the local deswollen region. The slower the transport of the solvent, the more significant the dip in $H$. Indeed, we see more significant dip for cases of lower $\Pi_0/G$, which is consistent with the slower relaxation observed at lower $\Pi_0/G$ in Fig. 5.

Next, we compare the simulation of different $K/G$ with fixed $\Pi_0/G = 10^{-2}$. Here the undrained limit at short time scale is unaffected by network compressibility (Fig. 6C). Only the

 

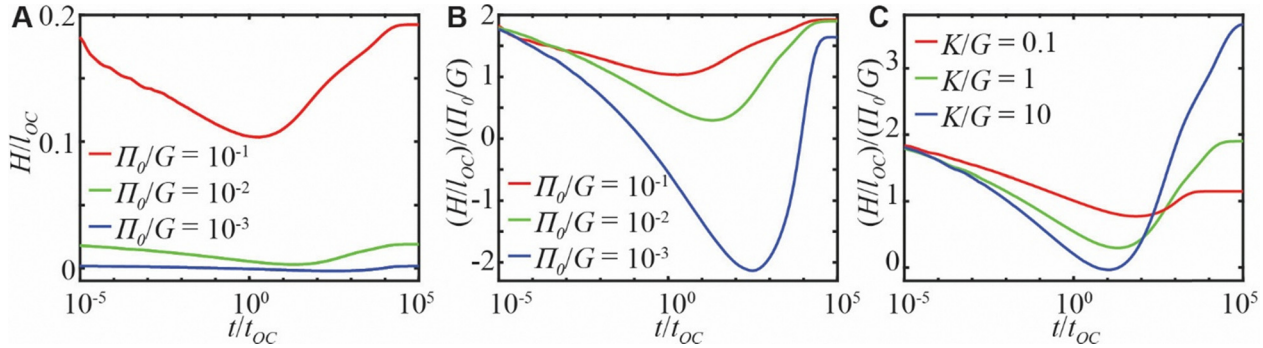


Fig. 6 How the height of surface elastic deformation evolves with time (A) fixing $K/G$ = 1, the elastic deformation increases with $\Pi_0/G$. (B) When $H$ is normalized by $\Pi_0/G$, cases of different $\Pi_0/G$ converge at the short-time undrained limit and the long-time drained limit. The case with lower $\Pi_0/G$ shows a larger dip in normalized $H$ due to slower solvent migration. (C) Fixing $\Pi_0/G = 10^{-2}$, the more compressible the network, the larger the deformation in the drained limit.

drained limit at long time scale is affected. It shows that the more compressible the network is, the easier it is to deform the solid in the drained limit. Also, the less compressible the network is (higher $K/G$), the less dip in $H$ in the intermediate time scale. If the network is fully incompressible, there would be a monotonic drop in $H$ with time, reflecting the decreasing capillary pressure as the size of osmocapillary phase separation increases.

## 7. Comparison with experiments

We compare the simulation results with the experimental data reported by Cai *et al.*[13] Cai *et al.* synthesized silicone elastomer swollen in silicone oils and used confocal microscopy to track the evolution of osmocapillary phase separation around a glycerol droplet. Both the swelling ratio of the elastomer and the molecular weight of the silicone oil have been varied to study their effect on osmocapillary phase separation. Their experiments showed that a less swollen elastomer leads to a smaller equilibrium volume of osmocapillary phase separation and faster relaxation. Since a less swollen elastomer has a higher osmotic pressure $\Pi_0$, the observation qualitatively agrees with our prediction that equilibrium osmocapillary phase separation size scales with $\gamma/\Pi_0$ and a higher $\Pi_0/G$ leads to faster relaxation (Fig. 5). Interested readers can refer to their original paper for these qualitative agreements. However, since the swelling-dependent osmotic pressure $\Pi_0$ and permeability $k$ were not measured, quantitative comparison of these trends is not possible.

To verify the $w \propto t^{0.32}$ scaling (Fig. 5) and the non-monotonic $H$–$t$ relation (Fig. 6), we focus on the relaxation data over the fully swollen elastomers measured by Cai *et al.*, which has the longest relaxation time, giving more data points to reflect the relaxation process. Cai *et al.* have measured the evolution of osmocapillary phase separation using silicone oil of three different molecular weights: 14 kg mol$^{-1}$, 28 kg mol$^{-1}$, and 49 kg mol$^{-1}$ (Fig. 7). They characterized the elastic deformation using the maximum vertical surface displacement relative to the initial undeformed surface, which is equivalent to $H$ discussed in Fig. 6. They characterized the size of osmocapillary phase separation by the vertical distance between the highest points of the solvent surface and the solid surface. This is equivalent to our phase separation height $h$ and is connected to the phase separation width $w$ by a constant as discussed in Section 4. Then their measurements can be directly compared to the simulated $w$ and $H$ discussed in Fig. 5 and 6. The deformation size for the 14 kg mol$^{-1}$ sample shows a clear decrease then increase behavior (Fig. 7A), agreeing with the behavior of $H$ in our simulation (Fig. 5). Since silicone

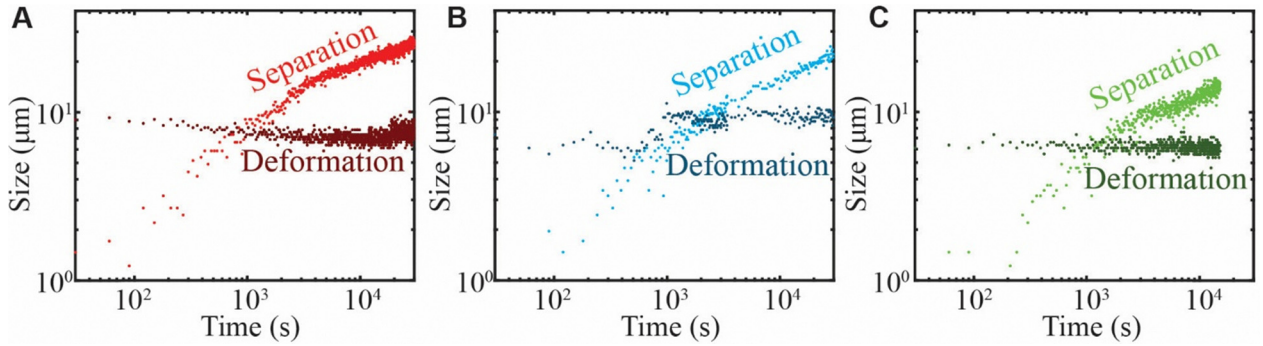


Fig. 7 The phase separation size (corresponding to our $w$) and the deformation size (corresponding to our $H$) measured by Cai *et al.*[13] for silicone oil of molecular weight (A) 14 kg mol$^{-1}$ (B) 28 kg mol$^{-1}$ (C) 49 kg mol$^{-1}$.

oil with higher molecular weight relaxes slower, samples with 28 kg mol$^{-1}$ (Fig. 7B) and 49 kg mol$^{-1}$ (Fig. 7C) did not show the increase in deformation size by the end of the measurement. The deformation size dominates over the phase separation at time scales shorter than $\sim 10^3$ s, indicating that nonlinear deformation is non-negligible at such time scales. The linear poroelastic modeling is only expected to be applicable at longer time scales.

To better compare the dynamic of phase separation with the simulated scaling law $w \propto t^{0.32}$, we plot the separation size of all samples in one plot (Fig. 8A). Two additional measurements of 14 kg mol$^{-1}$ and 49 kg mol$^{-1}$ samples are included. Since stress-free osmotic pressure $\Pi_0$ can easily change by orders of magnitude with a small change in solvent content near the fully swollen state (Fig. 3B), measurements of the same molecular weight show a variability comparable to that between measurements of different molecular weights. Nevertheless, all five sets of data follow the $w \propto t^{0.32}$ scaling at long time scales above $\sim 10^3$ s. Limited by the range of data, the difference between $w \propto t^{1/3}$ and $w \propto t^{0.32}$ cannot be experimentally distinguished. At short time scales, the nonlinear deformation is significant, and the relaxation is noticeably faster than $w \propto t^{0.32}$. For similar experiments, Qian *et al.* used $t^{1/2}$ to fit the relaxation in the short time scales.[18] Cai *et al.*'s data do not support the $t^{1/2}$ scaling at the short time scale. In Fig. 8A, relaxation keeps getting faster at shorter time scales. The $t^{1/2}$ power law can appear tangent to the relaxation data at intermediate time scales but is not an asymptote. The accelerated relaxation can be attributed to two nonlinear effects. First, if deformation induces significant surface curvature, the capillary pressure near osmocapillary phase separation pulls solvent towards the surface, accelerating the transport (Fig. 8B). Second, in the linear case, solvent flux into osmocapillary phase separation increases the curvature of the solvent surface, thus reducing the capillary pressure in the osmocapillary phase separation, which is the driving force for solvent migration. In the nonlinear case, the solvent flux is largely consumed by replacing the volume occupied by deformed solid without changing the surface curvature, thus not affecting the capillary pressure (Fig. 8C). Consequently, the driving force decreases slower, and overall relaxation is faster.

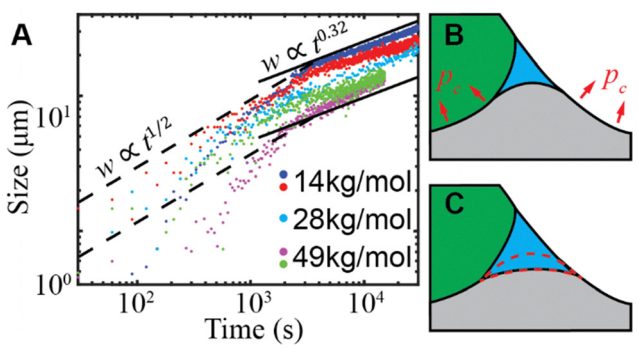


Fig. 8 Compare with experimentally measured growth dynamics of osmocapillary phase separation (A) experimental data agrees with the $w \propto t^{0.32}$ (solid black lines) scaling at long time scales when linear deformation assumption is valid. Relaxation is faster than both $t^{0.32}$ and the conventional $t^{1/2}$ (dashed black lines) at short time scales when nonlinear effect is significant. Same colors correspond to the same data set in Fig. 7. (B) With significant nonlinear deformation, capillary pressure on the surface promotes the solvent migration towards the surface, thus accelerating the relaxation. (C) With significant nonlinear deformation, the flux into the osmocapillary phase separation mainly fills the volume occupied by the deformed solid (encircled by red dashed line) rather than increasing the curvature of the solvent surface, thus not reducing the capillary pressure in the phase separation, leading to faster relaxation.

## 8. Summary

In summary, this paper developed the nonlinear and linear poroelastic model for dynamic osmocapillary phase separation. Finite element simulation based on the linear poroelastic model is performed to reveal how the relaxation of osmocapillary phase separation is affected by the compressibility of the network $K/G$ and the stress-free osmotic pressure $\Pi_0/G$. Both $K/G$ and $\Pi_0/G$ are connected to the swelling ratio of the polymer network through constitutive models such as the Flory–Rehner model. The simulation qualitatively agrees with experimental measurements on (1) a higher stress-free osmotic pressure $\Pi_0$ leads to faster relaxation and larger equilibrium size of osmocapillary phase separation. (2) The surface deformation induced by osmocapillary phase separation first decreases then increases with time. (3) The growth of the size of osmocapillary phase separation follows the $\propto t^{0.32}$ scaling when deformation is small. The linear model works at long time scales when $\Pi_0/G < 1$. At short time scales, the nonlinear deformation leads to non-power-law relaxation faster than $t^{0.32}$. For cases with $\Pi_0/G > 1$, the elastocapillary deformation dominates over osmocapillary phase separation. Consequently, the nonlinear effect is significant at all time scales. Since the size of osmocapillary phase separation is small and the wetting behavior is dominated by elastocapillary deformation when $\Pi_0/G > 1$, the poroelastic relaxation is likely dominated by the solvent migration within the swollen solid due to elastocapillary deformation,[32] rather than the osmocapillary relaxation that pulls the solvent out of the solid.

## Conflicts of interest

There are no conflicts to declare.

## Data availability

The work did not generate any experimental data. Necessary information to reproduce the simulation in the commercial software COMSOL has been included in the manuscript. An example simulation file using COMSOL 6.3 is provided in the supplementary information. See DOI: https://doi.org/10.1039/d5sm00993f.

 

# Appendices

## 1. Linearized Flory–Rehner model

At the reference state $\lambda_1 = \lambda_2 = \lambda_3 = \lambda_0$. Assume a small displacement field $u_i$ relative to this reference state. The deformation gradient $F_{iK} = \lambda_0\delta_{jK}(\delta_{ij} + u_{i,j})$. Plug into eqn (1) and (4):

$$\sigma_{ij} = \frac{Nk_BT}{\lambda_0^3(1+\varepsilon_{kk})}\left(\lambda_0^2\left(\delta_{ik}+u_{i,k}\right)\left(\delta_{jk}+u_{j,k}\right)-\delta_{ij}\right)-p\delta_{ij}. \quad \text{(A1)}$$

$$p = -\Pi - \frac{k_BT}{\Omega} \times\left[\log\left(1-\frac{1}{\lambda_0^3(1+\varepsilon_{kk})}\right)+\frac{1}{\lambda_0^3(1+\varepsilon_{kk})}+\frac{\chi}{\lambda_0^6(1+2\varepsilon_{kk})}\right] \quad \text{(A2)}$$

Here we have used eqn (5) to replace $\mu$ with $\Pi$ in eqn (4). Cancel out $p$ from eqn (A1) and (A2). The terms independent of $\varepsilon_{ij}$ gives the equilibrium condition at the new reference state:

$$\sigma_{ij} = \frac{Nk_BT}{\lambda_0^3}\left(\left(\lambda_0^2-1\right)\delta_{ij}\right)+\frac{k_BT}{\Omega}\left[\log\left(\frac{\lambda_0^3-1}{\lambda_0^3}\right)+\frac{1}{\lambda_0^3}+\frac{\chi}{\lambda_0^6}\right]\delta_{ij} + \varepsilon_{kk}\delta_{ij}+\Pi_0\delta_{ij}. \quad \text{(A3)}$$

The stress-free condition at this reference state ($\sigma_{ij} = 0$) requires:

$$\Pi_0 = -\frac{k_BT}{\Omega}\left[\log\left(1-\frac{1}{\lambda_0^3}\right)+\frac{1}{\lambda_0^3}+\frac{\chi}{\lambda_0^6}\right]-\frac{Nk_BT}{\lambda_0^3}\left(\lambda_0^2-1\right). \quad \text{(A4)}$$

Then the terms linear in $\varepsilon_{ij}$ gives:

$$\sigma_{ij} = 2\frac{Nk_BT}{\lambda_0}\left(\varepsilon_{ij}-\frac{\varepsilon_{kk}}{3}\delta_{ij}\right) + \left[\frac{Nk_BT}{3\lambda_0^3}\left(3-\lambda_0^2\right)+\frac{k_BT}{\Omega}\left(\frac{1}{\lambda_0^3-1}-\frac{1}{\lambda_0^3}-\frac{2\chi}{\lambda_0^6}\right)\right]\varepsilon_{kk}\delta_{ij}+\hat{\Pi}\delta_{ij}. \quad \text{(A5)}$$

Here $\hat{\Pi}$ is the deviation of the osmotic pressure from the reference state. Eqn (A5) are in the form of eqn (9) with $G$ and $K$ identified in eqn (10) and (11).

## 2. The geometry of osmocapillary phase separation

Consider the 2D phase separation drawn in Fig. 9. Under the assumption of osmocapillary phase separation dominating over the elastocapillary deformation, the swollen solid is negligibly deformed thus remaining flat. Then the geometry of the phase separation is solely determined by the interfacial tensions and the capillary pressure $p_C$ in the solvent (Fig. 9A). Here $\gamma$ is the solvent–air interfacial tension, $a$'s represent the dimensionless ratios between interfacial tensions, the subscripts S, G, L, A represent the solvent, gel, liquid, and air. For example, $a_{SL} = \gamma_{SL}/\gamma$. Denote the gel–solvent–liquid contact angle as $\theta_{SL}$ and the gel–solvent–air contact angle as $\theta_{SA}$. The force balance at these two three-phase contact lines follows the classical Young's equation:

$$a_{SL}\cos\theta_{SL} = a_{GS} - a_{GL}, \quad \text{(A6)}$$

$$\cos\theta_{SA} = a_{GS} - a_{GA}. \quad \text{(A7)}$$

At a length scale much larger than the osmocapillary phase separation, the apparent contact angle of the liquid droplet on the solid substrate is $\theta$ at the liquid–solvent–air contact line. The force balance over the whole solvent phase recovers the classical Young's equation:

$$a_{LA}\cos\theta = a_{GL} - a_{GA}. \quad \text{(A8)}$$

Introducing two auxiliary angles $\alpha$ and $\beta$, the force balance at this contact line gives:

$$a_{LA}\cos\theta = a_{SL}\cos\alpha - \cos\beta, \quad \text{(A9)}$$

$$a_{LA}\sin\theta = a_{SL}\sin\alpha + \sin\beta. \quad \text{(A10)}$$

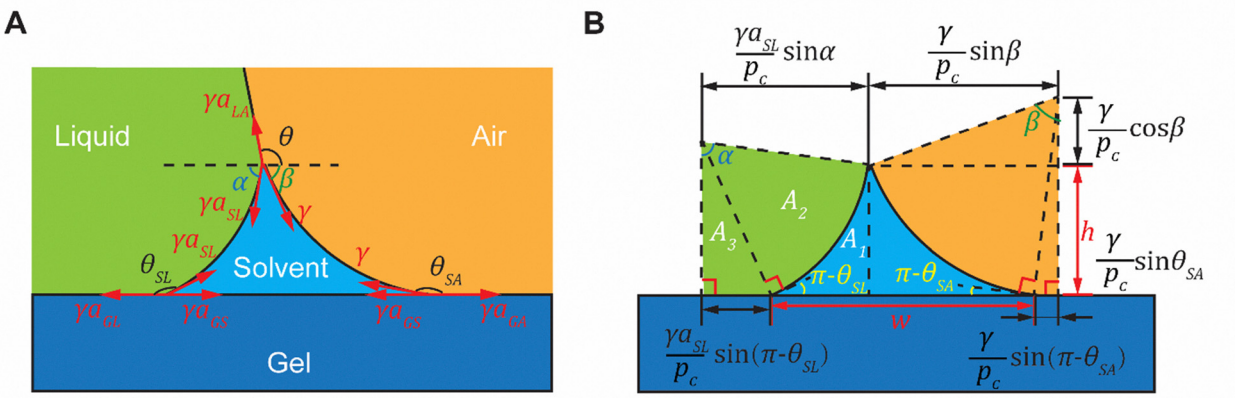


Fig. 9 (A) The interfacial tension between each phase ensures force balance. (B) The solvent–liquid and solvent–air interfaces have constant radius of curvature, allowing the geometry of the phase separation to be analytically predicted.

Eqn (A6)–(A10) allows the angles to be fully determined by the ratios between interfacial tensions:

$$\begin{aligned}\theta_{SL} &= \arccos\left(\frac{a_{GS}-a_{GL}}{a_{SL}}\right), \theta_{SA} = \arccos(a_{GS}-a_{GA}), \theta \\ &= \arccos\left(\frac{a_{GL}-a_{GA}}{a_{LA}}\right), \\ \alpha &= \arccos\left(\frac{a_{GL}-a_{GA}}{a_{LA}}\right) - \arccos\left(\frac{{a_{LA}}^2+{a_{SL}}^2-1}{2a_{LA}a_{SL}}\right), \\ \beta &= \arccos\left(-\frac{{a_{LA}}^2+1-{a_{SL}}^2}{2a_{LA}}\right) - \arccos\left(\frac{a_{GL}-a_{GA}}{a_{LA}}\right).\end{aligned} \tag{A11}$$

Eqn (A11) completely determines the shape of the phase separation. The size of the phase separation is determined by the length scale $\gamma/p_C$ where $p_C$ is the capillary pressure in the solvent phase. According to the Young–Laplace equation, the solvent–liquid and solvent–air interfaces are both circular arcs. Their radii of curvature are $a_{SL}\gamma/p_C$ and $\gamma/p_C$. Then according to the schematics in Fig. 9B, the phase separation height $h$ can be geometrically determined as $h = \gamma/p_C - \gamma/p_C \cos\beta$. Recalling the definition $h = C_h\gamma/p_C$, we have:

$$C_h = 1 - \cos\beta. \tag{A12}$$

The phase separation width $w$ can be determined as $w = (a_{SL}\gamma/p_C)(\sin\alpha - \sin\theta_{SL}) + (\gamma/p_C)(\sin\beta - \sin\theta_{SA})$. Recalling the definition $w = C_w\gamma/p_C$, we have:

$$C_w = a_{SL}(\sin\alpha - \sin\theta_{SL}) + \sin\beta - \sin\theta_{SA}. \tag{A13}$$

We assume the geometry has a unit in-plane depth, then we calculate the area of phase separation in Fig. 9B to represent the volume $V$. Consider the left half of the phase separation. The area of phase separation under solvent–liquid interface is denoted as $A_1$. Shape $A_1$, together with a fan-shape $A_2 = (a_{SL}\gamma/p_C)^2(\alpha + \theta_{SL} - \pi)/2$, and a triangle $A_3 = (a_{SL}\gamma/p_C)^2\sin(\pi - \theta_{SL})\cos(\pi - \theta_{SL})/2$, forms a trapezoid: $A_1 + A_2 + A_3 = ((a_{SL}\gamma/p_C)\cos(\pi - \theta_{SL}) + h)(a_{SL}\gamma/p_C)\sin\alpha/2$. $A_1$ is then calculated by subtracting $A_2$ and $A_3$ from the trapezoid. We can similarly derive the area of the right half of the phase separation. Then recalling the definition $V = C_V(\gamma/p_C)^2$, we have

$$\begin{aligned}C_V &= \frac{1}{2}\big[{a_{SL}}^2((-\cos\theta_{SL}+1-\cos\alpha)\sin\alpha \\ &\quad -(\alpha+\theta_{SL}-\pi)+\sin\theta_{SL}\cos\theta_{SL}) \\ &\quad +((-\cos\theta_{SA}+1-\cos\beta)\sin\beta \\ &\quad -(\beta+\theta_{SA}-\pi)+\sin\theta_{SA}\cos\theta_{SA})\big]\end{aligned} \tag{A14}$$

Note that all angular variables in eqn (A12)–(A14) can be expressed by the interfacial energies of the six interfaces involved, as eqn (A11) shows.

## Acknowledgements

This work is supported by National Science Foundation under grant no. 2337592. Any opinions, findings, and conclusions or recommendations expressed in this material are those of the authors and do not necessarily reflect the views of the National Science Foundation. The authors thank Dr Jonathan T. Pham for sharing the experimental data and helpful discussion on data interpretation.

## References

1 Q. Liu and Z. Suo, Osmocapillary phase separation, *Extreme Mech. Lett.*, 2016, **7**, 27–33.
2 J. Zhu and Q. Liu, The osmocapillary effect on a rough gel surface, *J. Mech. Phys. Solids*, 2023, **170**, 105124.
3 J. Zhu, C. Yang and Q. Liu, Experimental characterization of elastocapillary and osmocapillary effects on multi-scale gel surface topography, *Soft Matter*, 2023, **19**(45), 8698–8705.
4 L. Wang and Q. Liu, Deformation-dependent gel surface topography due to the elastocapillary and osmocapillary effects, *Soft Matter*, 2024, **20**(17), 3676–3684.
5 Q. Liu and L. Wang, Osmocapillary phase separation at the contact lines, *Soft Matter*, 2025, **21**, 6452–6457.
6 K. E. Jensen, R. Sarfati, R. W. Style, R. Boltyanskiy, A. Chakrabarti, M. K. Chaudhury and E. R. Dufresne, Wetting and phase separation in soft adhesion, *Proc. Natl. Acad. Sci. U. S. A.*, 2015, **112**(47), 14490–14494.
7 Z. Cai, A. Skabeev, S. Morozova and J. T. Pham, Fluid separation and network deformation in wetting of soft and swollen surfaces, *Commun. Mater.*, 2021, **2**(1), 21.
8 P. W. Wilson, W. Lu, H. Xu, P. Kim, M. J. Kreder, J. Alvarenga and J. Aizenberg, Inhibition of ice nucleation by slippery liquid-infused porous surfaces (SLIPS), *Phys. Chem. Chem. Phys.*, 2013, **15**(2), 581–585.
9 A. K. Epstein, T.-S. Wong, R. A. Belisle, E. M. Boggs and J. Aizenberg, Liquid-infused structured surfaces with exceptional anti-biofouling performance, *Proc. Natl. Acad. Sci. U. S. A.*, 2012, **109**(33), 13182–13187.
10 Z. Shao and Q. Liu, Osmocapillary adhesion: Reversible and strong adhesion between any hydrogel, *Extreme Mech. Lett.*, 2023, 101996.
11 X. Lou, Y. Huang, X. Yang, H. Zhu, L. Heng and F. Xia, External stimuli responsive liquid-infused surfaces switching between slippery and nonslippery states: fabrications and applications, *Adv. Funct. Mater.*, 2020, **30**(10), 1901130.
12 T. Josyula, L. Kumar Malla, T. M. Thomas, S. S. Kalichetty, P. Sinha Mahapatra and A. Pattamatta, Fundamentals and applications of surface wetting, *Langmuir*, 2024, **40**(16), 8293–8326.
13 Z. Cai, R. G. Badr, L. Hauer, K. Chaudhuri, A. Skabeev, F. Schmid and J. T. Pham, Phase separation dynamics in wetting ridges of polymer surfaces swollen with oils of different viscosities, *Soft Matter*, 2024, **20**(36), 7300–7312.

 

14 A. Hourlier-Fargette, A. Antkowiak, A. Chateauminois and S. Neukirch, Role of uncrosslinked chains in droplets dynamics on silicone elastomers, *Soft Matter*, 2017, **13**(19), 3484–3491.
15 A. Hourlier-Fargette, J. Dervaux, A. Antkowiak and S. Neukirch, Extraction of silicone uncrosslinked chains at air–water–polydimethylsiloxane triple lines, *Langmuir*, 2018, **34**(41), 12244–12250.
16 L. Hauer, Z. Cai, A. Skabeev, D. Vollmer and J. T. Pham, Phase separation in wetting ridges of sliding drops on soft and swollen surfaces, *Phys. Rev. Lett.*, 2023, **130**(5), 058205.
17 H. Jeon, Y. Chao and S. Karpitschka, Moving wetting ridges on ultrasoft gels, *Phys. Rev. E*, 2023, **108**(2), 024611.
18 W. Qian, W. Zhao, T. Qian and Q. Xu, Emergence and growth dynamics of wetting-induced phase separation on soft solids, *Phys. Rev. Res.*, 2024, **6**(3), 033210.
19 W. Hong, X. Zhao, J. Zhou and Z. Suo, A theory of coupled diffusion and large deformation in polymeric gels, *J. Mech. Phys. Solids*, 2008, **56**(5), 1779–1793.
20 P. Atkins and J. De Paula, *Physical chemistry*, Macmillan, 2006.
21 Z. Shao and Q. Liu, Independent characterization of the elastic and the mixing parts of hydrogel osmotic pressure, *Extreme Mech. Lett.*, 2023, 102085.
22 H.-J. Butt; K. Graf and M. Kappl, *Physics and chemistry of interfaces*, John Wiley & Sons, 2023.
23 R. W. Style, A. Jagota, C.-Y. Hui and E. R. Dufresne, Elastocapillarity: Surface tension and the mechanics of soft solids, *Annu. Rev. Condens. Matter Phys.*, 2017, **8**, 99–118.
24 B. Andreotti and J. H. Snoeijer, Statics and dynamics of soft wetting, *Annu. Rev. Fluid Mech.*, 2020, **52**(1), 285–308.
25 A. Pandey, B. Andreotti, S. Karpitschka, G. Van Zwieten, E. H. van Brummelen and J. H. Snoeijer, Singular nature of the elastocapillary ridge, *Phys. Rev. X*, 2020, **10**(3), 031067.
26 R. Masurel, M. Roché, L. Limat, I. Ionescu and J. Dervaux, Elastocapillary ridge as a noninteger disclination, *Phys. Rev. Lett.*, 2019, **122**(24), 248004.
27 H. Wang, *Theory of linear poroelasticity with applications to geomechanics and hydrogeology*, Princeton University Press, 2000.
28 A. R. Wufsus, N. Macera and K. Neeves, The hydraulic permeability of blood clots as a function of fibrin and platelet density, *Biophys. J.*, 2013, **104**(8), 1812–1823.
29 R. W. Balluffi; S. M. Allen and W. C. Carter, *Kinetics of materials*, John Wiley & Sons, 2005.
30 O. Coussy, *Poromechanics*, John Wiley & Sons, 2004.
31 K. L. Johnson, *Contact mechanics*, Cambridge University Press, 1987.
32 M. M. Flapper, A. Pandey, M. H. Essink, E. H. van Brummelen, S. Karpitschka and J. H. Snoeijer, Reversal of solvent migration in poroelastic folds, *Phys. Rev. Lett.*, 2023, **130**(22), 228201.